Biomacromolecules

Article

Cite This: Biomacromolecules 2019, 20, 3126−3141

pubs.acs.org/Biomac

Tailoring the Chemical Modification of Chitosan Hydrogels to Fine-Tune the Release of a Synergistic Combination of Chemotherapeutics

John D. Schneible,[†,§] Ankush Singhal,[‡,§] Radina L. Lilova,[†] Carol K. Hall,[†] Andrea Grafmüller,[*,‡] and Stefano Menegatti[*,†]

[†]Department of Chemical and Biomolecular Engineering, North Carolina State University, Raleigh, North Carolina 27695, United States

[‡]Department of Theory and Biosystems, Max Planck Institute for Colloids and Interfaces, Potsdam 14476, Germany

Supporting Information

ABSTRACT: Combination chemotherapy with a defined ratio and sequence of drug release is a clinically established and effective route to treat advanced solid tumors. In this context, a growing body of literature demonstrates the potential of hydrogels constructed with chemically modified polysaccharides as depots for controlled release of chemotherapeutics. Identifying the appropriate modification in terms of physicochemical properties of the functional group and its degree of substitution (χ) to achieve the desired release profile for multiple drugs is, however, a complex multivariate problem. To address this issue, we have developed a computational toolbox that models the migration of a drug pair through a hydrated network of polysaccharide chains modified with hydrophobic moieties. In this study, we chose doxorubicin (DOX) and Gemcitabine (GEM) as model drugs, as their synergistic effect against breast cancer has been thoroughly investigated, and chitosan as the model polymer. Our model describes how the modification of chitosan chains with acetyl, butanoyl, and heptanoyl moieties at different values χ governs both the structure of the hydrogel network and drug migration through it. Our experimental data confirm the in silico predictions for both single- and dual-drug release and, most notably, the counterintuitive inversion of release vs χ that occurs when switching from a single- to a dual-drug system. Consensus between predicted and experimental data indicates that acetyl modifications (χ = 32−42%) and butanoyl modifications (χ = 19−24%) provide synergistic GEM/DOX release molar ratios (i.e., 5−10). Collectively, these results demonstrate the potential of this model in guiding the design of chemotherapeutic hydrogels to combat cancer.

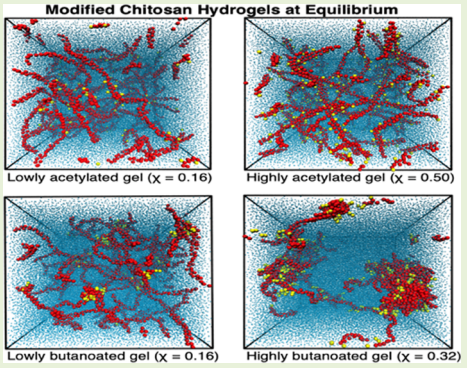

INTRODUCTION

Combination therapy with synergistic chemotherapeutics has become of increasing interest owing to its ability to overcome the main limitations of the single-drug approach: acquired drug resistance[1−3] and heavy dosage of highly cytotoxic drugs.[4,5] Multidrug chemotherapy operates by simultaneously disrupting various metabolic pathways in cancer cells and has been shown to overcome drug resistance and reduce side effects considerably.[6] The complementary action of drugs targeting different metabolic pathways, in fact, provides enhanced therapeutic activity while requiring a significantly lower dosage. Recent work in this field has demonstrated that the therapeutic outcome depends not only on the molar ratio of the drugs in the cocktail but also on the schedule of administration, that is, the sequence at which the various drugs reach the target cells.[7,8] Optimizing both ratio and sequence in a combined chemotherapy regimen is therefore essential to further lower the dosage relative to single-drug therapy needed to obtain a satisfactory therapeutic outcome.[7,9,10] This reduction of required therapeutic dosing (IC50 values) using drug combinations relative to single-drug chemotherapy has been recently demonstrated in vivo using various combination chemotherapy regimens and tumor models.[11−13]

To implement synergistic delivery schemes, researchers have investigated the use of nanoparticles,[8,11,14] liposomes,[15,16] micelles,[17,18] polymer−drug conjugates (PDCs),[12,19] and hydrogels.[20,21] Among these systems, hydrogels possess unique advantages. Owing to the flexible microstructure of hydrogels, release kinetics can be tuned by varying the gel fraction in physical hydrogels and the cross-linking density in chemically cross-linked gels.[22,23] In addition, hydrogels act as drug "depots" that afford sustained release and maintain a high local drug concentration in the surrounding tissues over an extended period, thereby circumventing the pharmacokinetic limitations of most chemotherapeutic agents.[24] Further, the loading and release rates of the therapeutic payload in and out of hydrogels are mostly governed by diffusion, which depend

Received: May 22, 2019
Published: July 16, 2019

DOI: 10.1021/acs.biomac.9b00707
Biomacromolecules 2019, 20, 3126−3141

on the molecular interactions between the polymer chains and the drugs, as well as the network morphology. These features have been harnessed for tuning the release kinetics and the scheduling of drugs, especially through chemical modification of the polymer backbone.[25]

A polymer of major interest to researchers and clinicians for developing therapeutic hydrogels is chitosan. Chitosan, which is derived from naturally abundant chitin, is a biocompatible, nontoxic polymer that is degradable by human enzymes.[26] In addition, the presence of primary amine groups on the glucosamine monomer provides a site for chemical modification, which has been extensively exploited to tailor the kinetics of drug release.[27,28] Interestingly, owing to their relatively short half-life in physiological media (i.e., days-month(s)), physical chitosan hydrogels are ideal for short-term delivery and do not release any toxic degradation byproducts.[29] As a result, a variety of chitosan-based formulations have been developed for oral, ophthalmic, and transdermal applications,[26,30−32] several of which have received FDA approval, demonstrating clear feasibility of these materials toward clinical translation.

Customizing the chemical modification of chitosan hydrogels to achieve a precise, synergistic ratio and kinetics of drug release, however, is a complex multivariate problem that depends on the physicochemical properties of the drugs, the composition and level of functional moieties, and the gel fraction. Collectively, these factors determine the hydrogel structure as well as the interactions between the drugs and the polymer backbone, thereby governing the release outcome. Such a large design space makes the optimization of hydrogels for the controlled release of specific combinations of chemotherapeutics extremely laborious. A toolbox capable of guiding the developmental phase would be of great assistance to pharmaceutical chemists in streamlining preclinical studies, thus realizing the full potential of these materials.

To this end, we have developed a method for guiding the chemical modification of chitosan chains to be utilized for designing hydrogels that afford the delivery for any desired drug combination with a synergistic molar ratio and kinetics. Our method comprises a computational modeling phase and an experimental validation phase. The computational phase comprises both all-atom and coarse-grained molecular dynamic (MD) simulations that model networks constructed with modified chitosan chains; its goal is to understand the microstructure/morphology, polymer−drug interactions, and the resulting diffusion of one or multiple drugs. The input design parameters input by the operator include (i) the chemical identity and distribution of the modifications across each chitosan chain, (ii) the ratios of the numbers of water molecules to polymer chains and of drug molecules to polymer chains, and (iii) the loading of the single drugs. While atomistic molecular dynamics can provide detailed insights into the effect of chemical modifications on the drugs' local interactions with the polymer chains, coarse-grained simulations enable rapid modeling of larger systems, containing a high number of polymer chains, water molecules, and drug molecules, for longer simulation times. Since the modeling of chemically modified, drug-loaded hydrogels requires simulations with sufficient spatio-temporal width to provide reliable guidance for design, we resolved to develop an ad hoc coarse-grained model.[33−35] Specifically, our model returns predicted diffusion coefficients of every drug species. The design parameters affording the most favorable diffusion coefficients toward synergistic molar ratio and kinetics of drug release were utilized in the experimental validation phase to construct the drug-loaded hydrogels.

To demonstrate our method, we selected doxorubicin (DOX) and Gemcitabine (GEM) as a model drug pair and three N-acyl groups (acetyl, butanoyl, and heptanoyl) as model modification moieties. The combination of DOX, a topoisomerase II inhibitor, and GEM, an antimetabolite, has been proven to be a highly effective drug regimen. Both are FDA-approved chemotherapeutics and have been studied in a variety of drug delivery vehicles, such as micellar nanoparticles, PDCs, polymersomes, mesoporous silica nanoparticles, and nanostructured lipid carriers.[15,36−40] Their synergistic combination has been demonstrated with multiple breast cancer cell lines, such as MCF7 and MDA-MB-231.[7,41] While extensive research has focused on their synergistic molar ratio, much less work has focused on the effect of scheduling on their therapeutic outcome. Vogus et al. have reported a strong effect of the scheduling of GEM and DOX release on MDA-MB-231 cells, by showing that simultaneous treatment with both drugs and incubation with GEM prior to DOX induced more toxicity than treatment with DOX prior to GEM, for the same concentrations. Furthermore, they showed that treatment with GEM prior to DOX (combination index, CI = 0.16 ± 0.03) afforded higher synergy than treating simultaneously with GEM and DOX (CI = 0.76 ± 0.10). They also found that the earlier the cells are exposed to GEM prior to DOX, the higher the resulting amount of synergy (lowest CI).[7] In a follow-up work, Vogus et al. studied the effect of the GEM:DOX molar ratio on MDA-MB-231 cells, and MCF-10a cells, non-tumorigenic breast epithelial cells, demonstrating that synergism on the cancer cells is fairly independent of molar ratio, whereas maximum antagonism to healthy cells occurs at the higher values of the molar ratio.[41] These studies provide evidence that an efficacious GEM/DOX delivery system should be able to stagger the release of the two drugs, such that GEM impacts the cells prior to DOX, and release a molar ratio of GEM:DOX > 1.

Acetyl, butanoyl, and heptanoyl moieties were chosen for chitosan modification as they represent similar but increasingly hydrophobic modifications and therefore allow us to study systematically the kinetics of drug release. Specifically, they enable two mechanisms of modulating the molar ratio and relative kinetics of drug release: the first based on the molecular interaction between modified chitosan chains and the drug molecules, and the second based on the formation of microscopic channels within the hydrogel network resulting from the hydrophobically driven aggregation of modified chitosan chains. The first mechanism applies mostly to hydrophobic drugs (e.g., DOX) resulting in slower release kinetics and becomes more prominent when the polymer is modified with longer aliphatic chains or with a higher degree of modification. The second mechanism, instead, impacts all drugs and depends not only on the composition and degree of modification but also on its distribution along the chitosan chain (e.g., random vs blocky). Both phenomena were captured by our coarse-grained molecular dynamics simulation and were observed experimentally with butanoyl- and heptanoyl-chitosan hydrogels.

The systems modeled and tested in this study feature chitosan hydrogels prepared with different degrees of modification (χ) (i.e., 0−50% molar acetyl, 5−40% molar butanoyl, and 5−30% molar heptanoyl on chitosan) and

DOI: 10.1021/acs.biomac.9b00707
Biomacromolecules 2019, 20, 3126−3141

loaded either with a single-drug (DOX or GEM) or with a double-drug (DOX and GEM) payload. We compared the predicted trends of drug diffusion coefficients with those obtained from experimental measures fitted on the Korsmeyer−Peppas equation.[42] Furthermore, we report the development of hydrogels that are capable of delivering the GEM/DOX combination with the desired kinetics and dose ratio of the pair. With dual-drug-loaded systems, acetyl-chitosan gels with χ = 32−42% delivered a GEM/DOX molar ratio of 7.5−10.5, whereas butanoyl-chitosan gels with χ = 19−24% delivered a molar ratio of 10−7.5. Further, the GEM/DOX ratio of release exponents calculated using the Korsmeyer−Peppas equation, which is a measure of release kinetics, was 3.7−8.9 for acetyl-chitosan gels and 5.6−6.3 for butanoyl-chitosan gels, indicative of faster GEM release than DOX. Both of these measures agree with computational results. Because the acetyl-modified gels display favorable release kinetics of GEM/DOX and a wider working range of modification, future work will further develop and test acetyl-modified gels for efficacy in vitro. Collectively, these results demonstrate the potential of the proposed strategy to guide the rapid, successful development of hydrogels—including, but not limited to, chitosan—for controlled release of synergistic combinations of anticancer drugs.

EXPERIMENTAL SECTION

Materials. Low-molecular-weight chitosan (85% maximum degree of deacetylation, 15 kDa) was obtained from Polysciences Inc. (Warrington, PA). Low-molecular-weight chitosan (75−85% degree of deacetylation, 50−190 kDa), acetic anhydride, phosphate-buffered saline (PBS), and the Kaiser Test kit were obtained from Sigma Aldrich (St. Louis, MO). Butyric and heptanoic anhydride were obtained from TCI Chemicals (Portland, OR). Doxorubicin hydrochloride (DOX) and Gemcitabine hydrochloride (GEM) were obtained from LC Laboratories (Woburn, MA). All other chemicals were of reagent grade or higher.

Modification of Chitosan. The protocol of chemical modification of chitosan was adapted from Kubota et al.[43] Briefly, chitosan was dissolved in 1% wt acetic acid (aq) at a concentration of 6 mg/mL and filtered to remove insoluble components. A stoichiometric amount of chosen anhydride (acetic, butyric, or heptanoic) was added to the chitosan solution and allowed to react at room temperature overnight. The solution was then precipitated by dropwise addition in a 3× reaction volume of 5 M methanolic potassium hydroxide. The precipitate was then collected and washed to neutral pH with methanol and copiously washed with water to yield a physical hydrogel. The gel was weighed, and subsequently lyophilized and weighed, to determine the gel fraction as the ratio of the mass pre and post lyophilization.

Determination of the Level of Modification. The level of acyl modification of the chitosan polymer chains was measured using a modified version of the Ninhydrin assay developed by Kaiser et al.[44] Briefly, lyophilized samples of modified chitosan were dissolved in 1% acetic acid (aq) at 3 mg/mL, and native chitosan (used to generate a standard curve) was dissolved at varying concentrations (0.5−7.5 mg/mL). Chitosan solutions were then combined with 30 μL of potassium cyanide in water/pyridine and ninhydrin and 6% in ethanol. The solutions were then incubated at 100 °C for 5 min. The solution was then diluted to 20×, and absorbance at 570 nm was measured by UV−vis spectroscopy. The level of modification was determined through the derived eq 1

$$\chi = \frac{\left(1 - \frac{\bar{C}DM_{\text{monomer}}}{C}\right)}{\left(1 - \frac{\bar{C}DM_{\text{modification}}}{C}\right)} \quad (1)$$

where χ is the degree of modification, $\bar{C}$ is the molar concentration of amine groups on a chitosan chain, D is the dilution factor, C is the mass concentration used for the Kaiser test, M_{monomer} is the molecular weight of the glucosamine monomer, and $M_{\text{modification}}$ is the molecular weight of the modification (acetyl, butanoyl, or heptanoyl).

Computational Procedure. The simulations were performed utilizing the GROMACS 4.6.4 package.[45] All-atom molecular dynamics (MD) simulations were performed using the GLYCAM-$M^{TIP5P}_{OSMOr14}$ force field.[46,47] The parameters for the butanoyl and heptanoyl modifications, as well as for GEM and DOX were obtained from the gaff force field,[48] whereas the partial charges were derived following the GLYCAM06 protocol.[46] All all-atom chitosan systems contained 10 chitosan chains with degree of polymerization (DP, number of monosaccharides per chain) of 16, and 200 water molecules per chain. Separate simulations were performed using 50 DOX, 50 GEM, or 50 DOX and 50 GEM molecules, with 10 water molecules per drug molecule, to derive the interaction potentials for the drug−drug and drug−water interactions. Similarly, additional systems containing 10 DOX or 10 GEM molecules together with 10 chitosan chains with DP = 16 and 200 water molecules per chain were simulated to derive the drug−polymer interaction. The particle mesh Ewald method[49] was used to calculate the long-range electrostatic interaction using a Lennard-Jones (LJ) and electrostatic interaction with a cutoff of 1.4 nm. The system was equilibrated in the NPT ensemble for 50 ns using a Parinello−Rahman barostat with additional pressure dispersion correction[50] and subsequently equilibrated for 400 ns in the NVT ensemble. A final 100 ns NVT MD simulation was performed to derive the coarse-grained interaction potentials.

In the coarse-grained model, each monosaccharide was mapped onto three coarse-grained interaction sites. The modifications were represented by one, two, and three additional sites for the acetyl, butanoyl, and heptanoyl groups, respectively. Water molecules were represented as a single coarse-grained site. DOX and GEM were represented by 11 and 4 coarse-grained sites, respectively. The interaction potentials between these sites were generated using Boltzmann inversion[51] for the bonded interactions and the MSCG method[52] for nonbonded interactions, following the procedure described by Sauter et al.[53] Coarse-grained systems containing 20 chitosan chains with DP of 50, and 100 000 water beads (5000 water molecules per chains), were equilibrated for 100 ns using the Nosé−Hoover thermostat.[54−56] The drug diffusion simulations were performed by randomly loading the chitosan networks with either 10 DOX or 10 GEM for single-drug release or 10 DOX and 10 GEM molecules for dual-drug release. The diffusion coefficients of the drugs were obtained from the slope of their mean square displacement (MSD) as a function of time. Pore distributions were calculated using the procedure described by Bhattacharya and Gubbins[57] with the SOLVOPT routine for constrained nonlinear optimization.[58] The procedure finds the largest sphere that can be placed in the network while containing randomly chosen points.

Single-Drug Loading and Release Studies. Initial single-drug loading and release studies were performed using low-molecular-weight chitosan (Polysciences Inc). Drug loading experiments were performed by incubating 150 mg of chitosan hydrogel with 1 mL of a 1 mg/mL aqueous drug solution for 48 h. After loading, the drug-depleted supernatant was collected for drug quantification by UV−vis spectroscopy. The loaded hydrogel was then combined with 1 mL of 0.01 M PBS pH 7.4 and placed in a 37 °C orbital shaker at 50 rpm. At selected time points, 200 μL of the sample was withdrawn and replenished with fresh PBS. After the release studies, all samples (loading supernatant and time point collections) were analyzed by UV−vis on Biotek Synergy at 480 and 290 nm to determine the amounts released of DOX and GEM, respectively.

Dual-Drug Loading and Release Studies. Dual-drug loading and release studies were performed on the low-molecular-weight chitosan gels Polysciences Inc. Samples of 150 mg of hydrogel were incubated with 1 mL of a 1 mg/mL aqueous DOX/GEM solution, 50/50 molar ratio, for 48 h. The supernatant was collected, and the loaded hydrogel was then combined with 1 mL of 0.01 M PBS pH 7.4

DOI: 10.1021/acs.biomac.9b00707
Biomacromolecules 2019, 20, 3126−3141

and placed in a 37 °C orbital shaker at 50 rpm. At selected time points, 200 μL of the aqueous supernatant was withdrawn and replenished with fresh PBS. Samples were then passed through a Waters 2690 Separation reversed-phase high-performance liquid chromatography system equipped with an Aeris 3.6 μm C18 column (150 × 4.6 mm). The gradient utilized 0.1% formic acid (A) and acetonitrile with 0.1% formic acid (B) from 5−100% B over 10 min. The column eluate was monitored at wavelengths of 290 and 480 nm, wavelengths corresponding to the GEM and DOX. The concentrations of GEM and DOX were determined by peak-area integration of the resulting 290 and 480 nm chromatograms relative to the respective standard curves.

Mathematical Drug Release Models. Several models are used to describe drug diffusion profiles[59] or the quantity of drug released from the modified chitosan hydrogels over time (Supporting Information, Table S2): (i) the zero-order model, which describes drug dissolution from pharmaceutical dosage forms that do not disaggregate and release the drug slowly; (ii) the first-order model, which describes drug dissolution that occurs from porous matrices and water-soluble drugs; (iii) the Hixson−Crowell model,[60] which describes release that occurs in planes that are parallel to the drug surface if the tablet dimensions diminish proportionally, meaning that the initial geometrical form keeps constant all the time; (iv) the Higuchi model,[61] which describes the release of water-soluble and low-solubility drugs incorporated in semisolid and/or solid matrixes; and (v) the Korsmeyer−Peppas model,[42] which characterizes release from hydrophilic matrices and is presented in eq 2

$$\frac{Q_t}{Q_\infty} = K_k t^n \tag{2}$$

where Q_t is the amount of drug released at time t, Q_∞ is the maximum possible amount, and the ratio of Q_t to Q_∞ is the percent release. K_k is the release rate constant, which is correlated to the diffusion coefficient, and n is the release exponent, where $n \sim 0.5$ denotes Fick-type drug diffusion, and $n > 0.5$ indicates that spatial rearrangement of the polymer chains also contributes to drug transport. The release exponent, n, is a metric for characterizing the mechanism of release. To determine n, only the portion of the release curve where $Q_t/Q_\infty < 0.6$ was used. The in vitro drug release data was analyzed by fitting it to all models listed in Table S2.

RESULTS AND DISCUSSION

Chitosan Gel Preparation and Selection. Initial studies were performed using two chitosan starting materials to evaluate the properties of the resulting gels, namely, the consistency in gel fraction across different acyl modifications and different degrees of modification and to select a polymer for further optimization. Figure 1 illustrates the polymer gel fraction (i.e., the mass of polymer contained in a given mass of hydrogel) obtained with either 15 or 50−190 kDa chitosan using acetyl, butanoyl, and heptanoyl moieties, spanning a wide array of modification levels, ranging from native chitosan (0% modified) to 50% modified. Interestingly, the gel fraction was found to depend only on the acyl moiety used to modify the polymer but not on the chitosan molecular weight. The mean gel fractions (percent ratio of polymer weight vs total hydrogel weight) obtained with 15 kDa chitosan (~90 monomers), in fact, were 2.02 ± 0.5, 2.59 ± 0.3, and 3.31 ± 0.4 for the acetyl-, butanoyl-, and heptanoyl- modifications, respectively, whereas the corresponding values obtained with 50−190 kDa chitosan (~300−1200 monomers) were 2.14 ± 0.6, 2.63 ± 0.2, and 3.29 ± 0.5, across all modification levels. This consistency in gel fraction across a vastly different length of polymer suggests that the physical behavior of the gels depends mainly on the type and degree of the modification groups. Thus, to maintain consistency between the experimental and in silico studies,

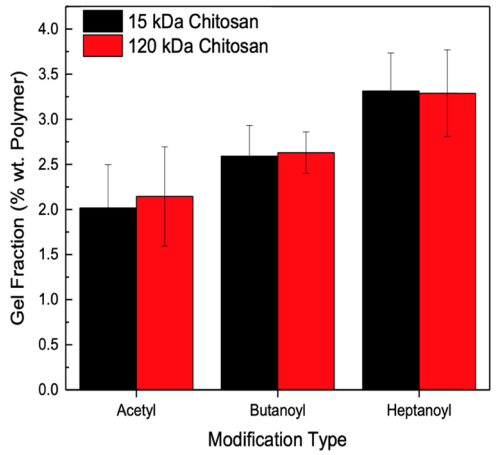

Figure 1. Comparison of gel fraction for acetyl-, butanoyl-, and heptanoyl-chitosan gels prepared using base chitosan polymers with molecular weights of 15 and 50−190 kDa. Data represent mean ± 95% CI ($n \geq 12$).

which are limited to 50 monomer-long chitosan chains to limit computational costs, 15 kDa chitosan was utilized in all subsequent studies. With the drug transport through the hydrogels being dependent on both gel fraction and modification on the polymer backbone, consistency in gel fraction values is critical to study the correlation between drug release and the type and degree of modification. Since the gel fraction for heptanoyl-modified gels was statistically different from acetyl-modified gels, and the average gel fraction values for acetyl- and butanoyl-modified gels were closer than those of butanoyl- and heptanoyl-modified gels with both 15 and 50−190 kDa chitosan, drug release from heptanoyl-modified hydrogels was not computationally modeled, and the experimental data are reported in the Supporting Information.

In Silico Modeling of Single and Dual-Drug Diffusion through Modified Chitosan Hydrogels. *Drug−Chitosan Interactions at All-Atom Resolution.* All-atom simulations of the drug-loaded chitosan hydrogels were analyzed to obtain a molecular-level understanding of (i) the interactions between the drug molecules and the modified chitosan chains and (ii) the dependence of these interactions on the type and degree (χ) of modification. Atomistic systems feature a high density of saccharide monomers (chitosan) and low water content, which is necessary to obtain a sufficient sampling of the forces needed to implement the coarse-grained procedure. This high density, however, results in many nonbonded interactions between the polymer and drug molecules. It must be also noted that the frequency of these interactions in real hydrogels, where the water content is much higher, is much lower. Nonetheless, the atomistic analysis of these interactions provides insight into their relative contribution toward determining drug diffusion through the network. The interaction energies among the drug molecules, the chitosan backbone, and the modification groups were separated into electrostatic and Lennard-Jones (LJ) contributions and the ability to form hydrogen-bond contacts. The resulting interactions between DOX and modification groups and between DOX and the chitosan backbone as a function of χ are reported in Figure 2. The analogous results for GEM are reported in Figure S1. The hydrogen-bond interactions for DOX modification and DOX backbone as a function of χ are reported in Figure S2.

DOI: 10.1021/acs.biomac.9b00707
Biomacromolecules 2019, 20, 3126−3141

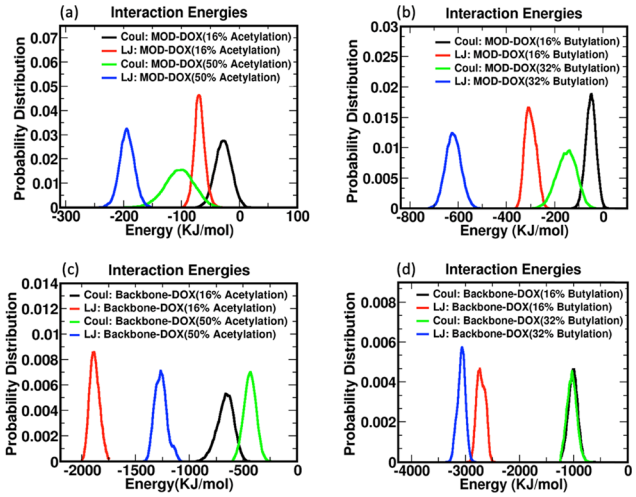

Figure 2. Lennard-Jones and Coulombic contribution to the DOX-modification group interaction energy for (a) acetyl-chitosan and (b) butanoyl-chitosan; and Lennard-Jones and Coulombic contribution to the DOX-backbone interaction energy for (c) acetyl-chitosan and (d) butanoyl-chitosans at different χ.

We observed that the interactions between drug molecules and modified chitosan chains were consistently of the LJ type, particularly for DOX, which interacts both with the chitosan backbone and with the modification groups. The daunosamine moiety in DOX aligns with the pyranose rings in the chitosan backbone, resulting in the formation of multiple hydrogen bonds (Figure S3). As χ increases, the number of contacts (nonbonded interactions) between DOX and the modification groups (both acetyl and butanoyl) increases, resulting in higher interaction energy as shown in Figure 2. On the other hand, the dependence of the backbone interactions with χ is less clear, as the number of nonbonded interactions decreases with χ for acetyl modifications and increases slightly for butanoyl modifications. It should be noted, however, that DOX molecules tend to aggregate into clusters, thereby reducing their ability to form interactions with the backbone, especially within the time scale of the all-atom simulations, where equilibration of the aggregate size is not accessible. GEM shows overall weaker interactions with the modified chitosan chains compared with DOX. The LJ contribution to the interaction energy, in fact, is about 50% of that observed with DOX, whereas the electrostatic contribution is approximately the same for the two drugs.

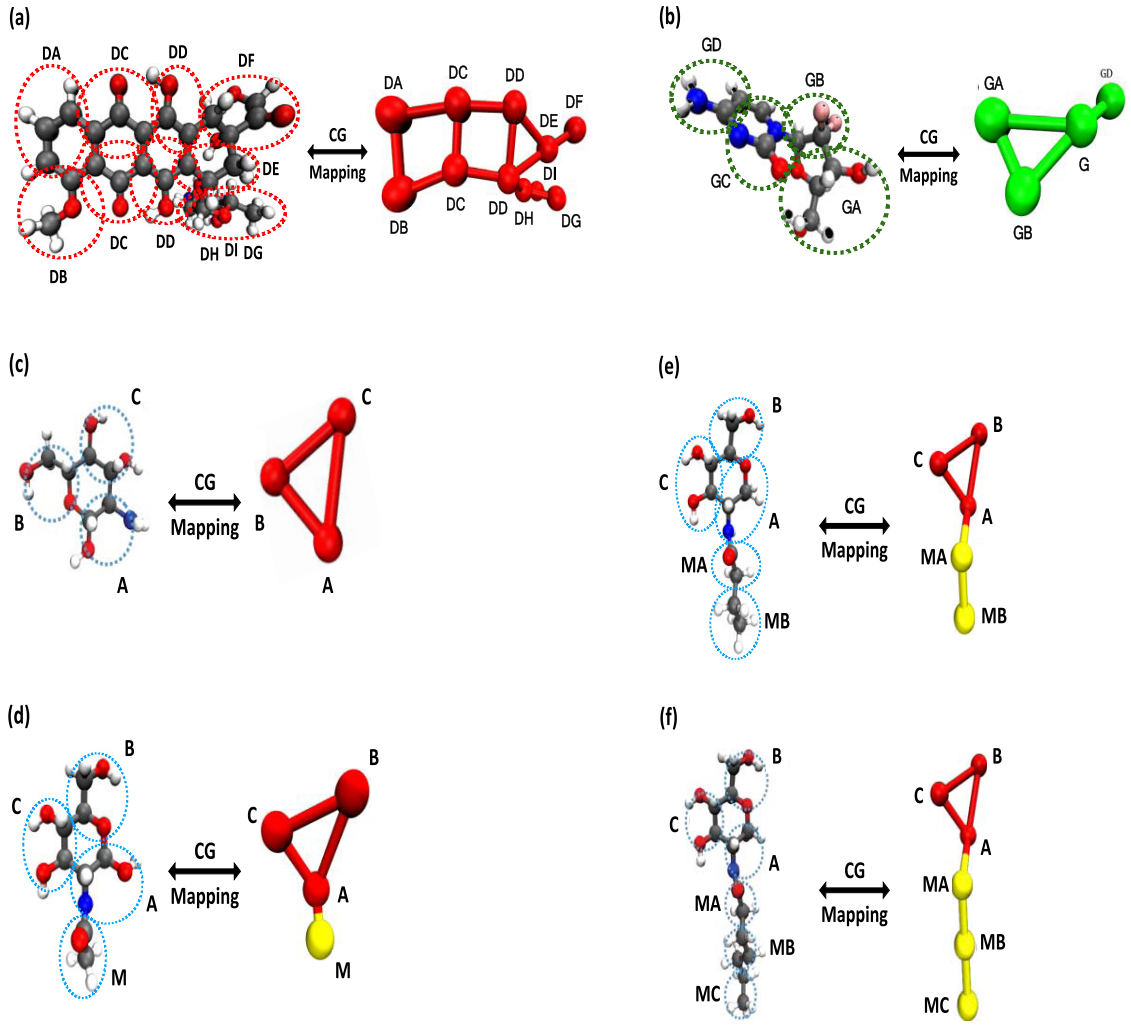

Figure 3. All-atom and coarse-grained representations of (a) DOX, (b) GEM, (c) unmodified glucosamine monomer, (d) acetyl-glucosamine, (e) butanoyl-glucosamine, and (f) heptanoyl-glucosamine.

DOI: 10.1021/acs.biomac.9b00707
Biomacromolecules 2019, 20, 3126−3141

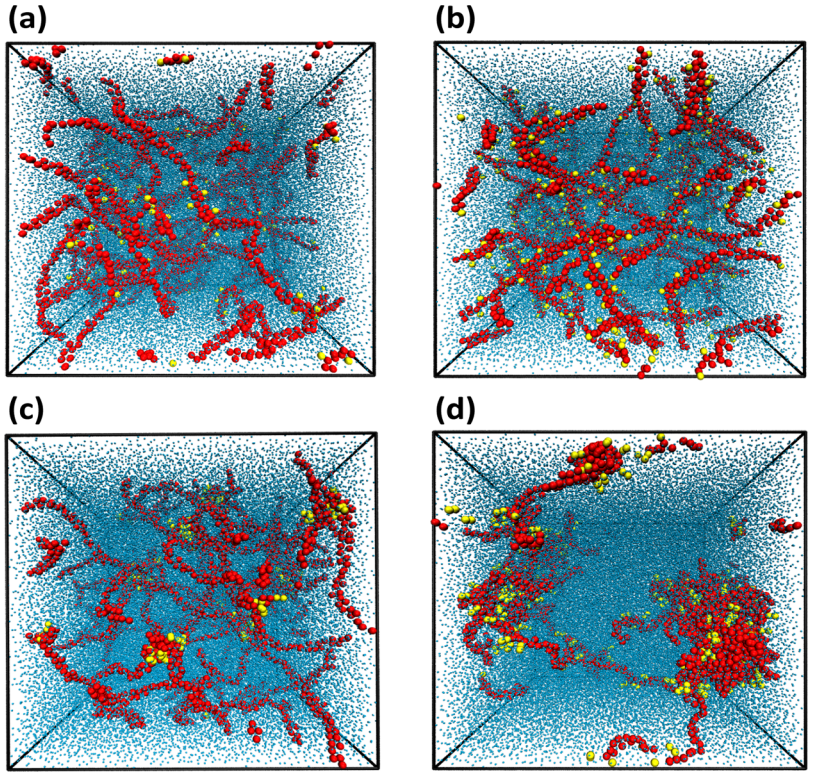

Figure 4. Representative simulation snapshots of chitosan hydrogels with a blocky modification pattern for (a) 16% acetylation, (b) 50% acetylation, (c) 16% butanoation, and (d) 32% butanoation.

Coarse-Grained Simulations of Acyl-Modified Chitosan Hydrogels. The all-atom simulations described in the last section were performed to evaluate the molecular-level interactions and elucidate the thermodynamic mechanisms by which the drugs interact with the chitosan backbone and the modification groups. However, to understand how the chemical modifications govern the morphology of the hydrogel and the transport of the drugs therein, it is necessary to model drug-loaded hydrogels across a large spatio-temporal scale, where a high number of elements (long polymer chains, drug molecules, and water molecules) and their dynamic interplay can be simulated, thereby rendering a physically accurate representation of these systems. This, however, is not possible with all-atom simulations. We therefore resolved to adopt a coarse-grained modeling procedure that was informed by the results of the all-atom simulations and that has been shown to capture the behavior of the polysaccharide-based hydrogel.[47]

The coarse-grained models for the base glucosamine and the modified (acetyl, butanoyl, and heptanoyl) glucosamine monomers, as well as the drug molecules were constructed as routinely done by grouping four heavy atoms into one coarse-grained interaction site while preserving the overall ring topology of the molecule. Water molecules were represented by one coarse-grained interaction site. The coarse-grained mapping of GEM and DOX is shown in Figure 3a,b, whereas that of the monosaccharides with zero, one, two, and three interaction sites corresponding to unmodified and acetyl, butanoyl, and heptanoyl modifications is reported in Figure 3c–f.

The coarse-grained interaction potentials of the drug molecules and the chitosan chains were obtained from all-atom molecular dynamics (MD) simulations following the force matching method[62−64] and a procedure outlined in our prior work.[53] The radial distribution functions between all interaction sites of the coarse-grained model showed excellent agreement with their equivalent obtained from all-atom simulations as shown in Figure S4. The transferability to systems with different degrees of modification was explicitly confirmed so that the coarse-grained model was expected to accurately reflect the interactions of the underlying atomistic force field.

The hydrogel models were set to comprise 20 chitosan chains, each of 50 monomers (polymerization degree, DP = 50), and modified using the same values of χ utilized in the follow-up experimental work: χ of 0, 16, 32, and 50% for acetyl-chitosan, and χ of 0, 16, 24, and 32% for butanoyl-chitosan.

We considered the use of chitosan chains with DP > 50 unnecessary, given the lack of correlation between the gel fraction and the molecular weight of chitosan (Figure 1) and the resulting higher computational cost. Furthermore, the modification pattern, that is, the distribution of the acetyl-, butanoyl-, and heptanoyl- groups on the chitosan chains, was also considered. In real hydrogels, both χ and the modification patterns are governed by the monomers and the reagents utilized for chemical modification, as well as the structure of the polymer chain in solution as it evolves through the course of the chemical modification. Whereas χ can be easily measured, evaluating the modification patterns is much more challenging, and it is often assumed to be random. However, other distributions of the modification groups resembling either an evenly spaced or a blocky pattern can also be envisioned, and their presence can be inferred based on indirect measurements derived from macroscopic behaviors of the polymer. A consideration for the modified chitosan molecules is that the hydrophobic tails (acetic, butanoic, and

DOI: 10.1021/acs.biomac.9b00707
Biomacromolecules 2019, 20, 3126−3141

heptanoic) of the anhydrides utilized for modifying the chitosan chains dissolved in an acidic aqueous environment are likely to aggregate around the modified monomers that are initially formed and promote localized modification thereupon, resulting in a block-type pattern.

Both χ and the modification pattern, in fact, govern the aggregation of polymer chains in solution; in particular, chain aggregation is promoted by blocky modification patterns as opposed to a random distribution along the polymer chain.[65−67] To evaluate the effect of the modification pattern on the network structure and molecular interactions, chitosan chains modified with two different patterns, namely, evenly spaced (i.e., two neighbor modification groups are separated by a number of unmodified monomers equal to $[PD(1 - \chi)]/[PD\chi - 1]$) and blocky (i.e., clusters of MM modified monomers separated by a number of unmodified monomers equal to $[MM(1 - \chi)]/\chi$), were constructed to be simulated. A random modification pattern, where blocks of different sizes are assigned to every chain, would render the derivation of structure vs χ correlations particularly challenging and was not considered in this work. The hydrogels were constructed with 100 000 water molecules in total, corresponding to a gel fraction value of 8.2%. While this is higher than the experimental values (2−2.5% wt), increasing the number of water molecules per polymer chain would escalate the computational costs and prevent the possibility of scanning over a range of conditions for system optimization. The resulting equilibrated structures of acetyl- and butanoyl-chitosan featuring blocky modification pattern are presented in Figure 4, whereas the corresponding structures with an evenly spaced modification pattern are reported in Figure S5.

The coarse-grained simulation of these systems indicates that increasing χ consistently promotes aggregation of the chitosan chains, morphing the microstructure of the gel from a homogeneous network of contacting chains to a heterogeneous system featuring hydrophobic-rich domains (clusters) surrounding large pores (channels). This transition is evident with butanoyl-chitosan, which shows a strong dependence of aggregation upon the modification pattern (see Figure 4c,d for a blocky modification pattern with χ = 16 and 32%, respectively, and Figure S5c,d for an evenly spaced pattern with χ = 16 and 32%, respectively), and a less pronounced dependence upon the modification pattern for acetyl-chitosan, for which both the modification pattern and the value of χ seem to have little or no influence (see Figure 4a,b for the blocky modification pattern with χ = 16 and 50%, respectively, and Figure S5a,b for the evenly spaced pattern with χ = 16 and 50%, respectively). The clusters formed at high values of χ feature a hydrophobic core, which comprises the segments of chitosan chains carrying the modification, and a hydrophilic shell; polymer bridges connecting the clusters are formed by the chitosan segments carrying low or no modification. These types of structures (Figure 5) have been extensively studied in prior literature and have been comprehensively reviewed by Philippova and Korchagina.[68]

To obtain a more quantitative measure of network homogeneity, the structures derived from the coarse-grained simulations were analyzed by calculating the distribution of pore sizes (Figure 6). The pore size distribution in the acetyl-chitosan network remains essentially unchanged over the entire range of χ for both evenly spaced and blocky modification patterns (Figure 6a,b); this corresponds to the homogeneous network structure featuring relatively small pores shown in the simulation snapshots in Figure 4a,b. In butanoyl-chitosan, on the other hand, the pore size distribution shifts to markedly larger pore diameters at higher χ, indicating the appearance of large channels resulting from the formation of hydrophobic clusters for both modification patterns. The comparison between pore size distributions further indicates that the transition of butanoyl-chitosan from a homogeneous network to cluster/channel morphology occurs at lower χ with a blocky modification pattern than with an evenly spaced pattern (Figure 6c,d). The large difference in the hydrogel morphology between acetyl and butanoyl modifications likely plays a significant role in determining the migration of drug molecules.

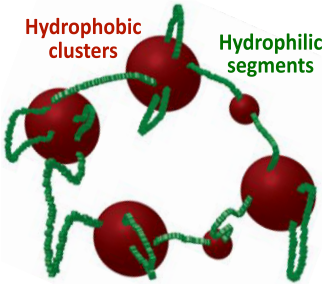

Figure 5. Schematic cluster/channel structure formed by hydrophobically modified chitosan, wherein the micellar aggregates (red) comprise chitosan segments with a high degree of hydrophobic modification, and the bridges (green) represent chitosan segments with a low degree of modification.[68]

Simulation of Single-Drug Migration through Modified Chitosan Hydrogels. After equilibrating the chitosan hydrogel structure, the coarse-grained hydrogels were loaded with 10 drug molecules of either DOX or GEM initially placed at random positions. The number of drug molecules was chosen to match the loading (ratio of drug molecules vs polymer chains) featured by the experimental systems. In choosing the number of drug molecules, we also considered the tradeoff between ensuring reproducible simulations (higher drug loading) and avoiding the formation of aggregates (lower drug loading). While, in fact, an insufficient number of drug molecules can lead to poor statistical significance, especially when diffusing through structurally nonhomogeneous systems, excessive drug loading results in the formation of aggregates, which would distort drug migration through the polymer network. Regarding the choice of distributing the drug molecules randomly across the network, we note that the diffusion constants obtained by arranging the drug molecules into different initial distributions showed the same trends and, in most cases, agree within the fitting error.

Coarse-grained simulations of 10 ns were performed, and the migration of the drug molecules through the networks was monitored. The diffusion constants were calculated from the slope of the mean-squared displacement (MSD) of the drug molecules with respect to time and are reported in Figure 7; it should be noted that the diffusion constants did not significantly change with simulations performed at longer time scales. The error bars correspond to the fitting error due to the nonlinearity of MSD fitting.

As anticipated, the differences in hydrogel morphology (homogeneous vs clusters/channels) and physicochemical properties of the drugs and the modification groups result in different trends of drug diffusion vs χ. GEM migrates through all networks with a diffusion constant similar to that of free GEM in water, indicating that there is no effect of the polymer

DOI: 10.1021/acs.biomac.9b00707
Biomacromolecules 2019, 20, 3126−3141

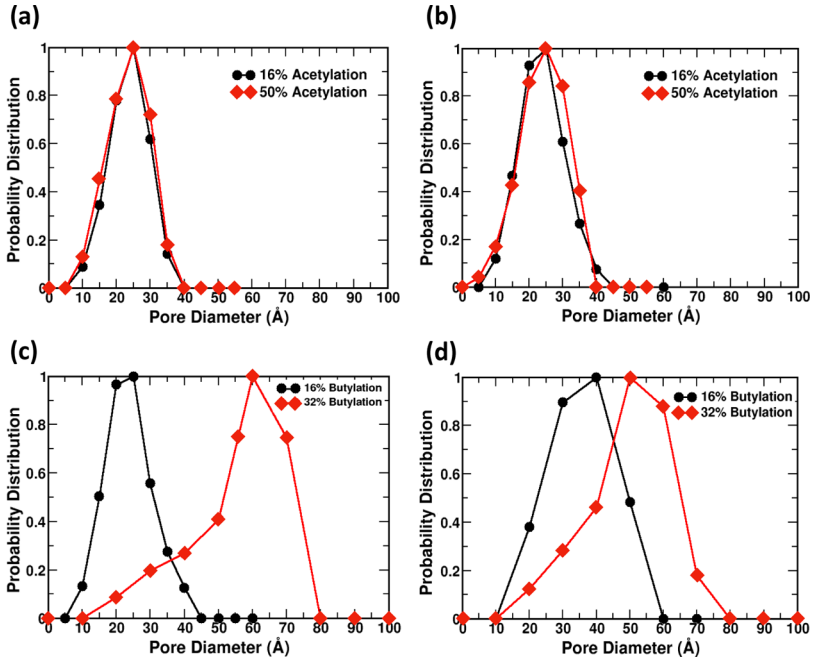

Figure 6. Pore size distribution functions for (a) evenly spaced acetyl-chitosan, (b) blocky acetyl-chitosan, (c) evenly spaced butanoyl-chitosan, and (d) blocky butanoyl-chitosan.

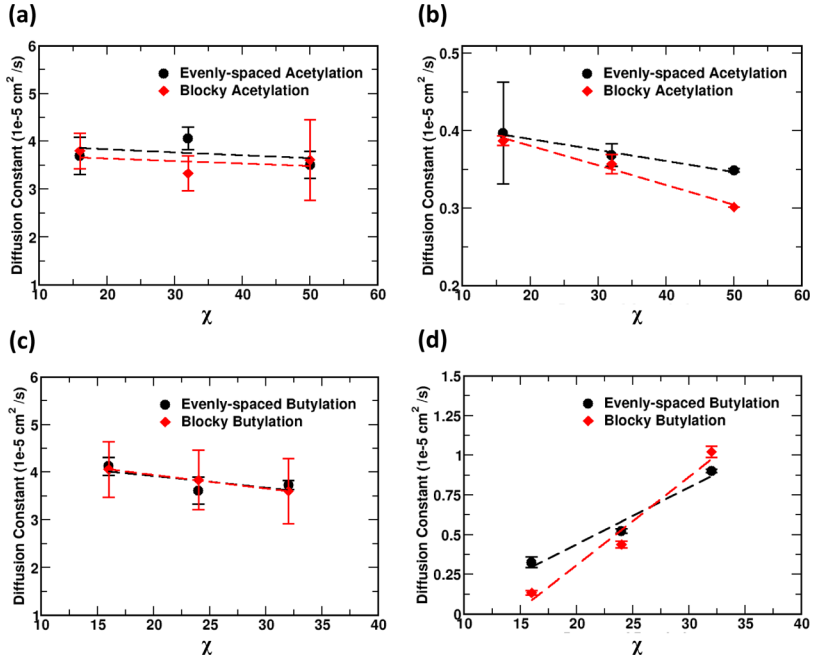

Figure 7. Drug diffusion constants vs χ for single-drug migration across different chitosan networks for evenly spaced (black) and blocky (red) modification patterns: (a) GEM and (b) DOX in acetyl-chitosan, and (c) GEM and (d) DOX in butanoyl-chitosan.

on its diffusion (Figure 7a,c). GEM molecules, which are small and hydrophilic, form a relatively low number of nonbonded interactions with the chitosan chains, irrespective of the type of modification and χ, as listed in Table S1. Owing to the limited interaction with the polymer chains, GEM travels easily through the water-filled channels in both homogeneous and cluster/channel hydrogel morphologies. Only a slight reduction in GEM diffusion is observed in butanoyl-chitosan at higher χ.

On the other hand, DOX molecules, which are larger and more hydrophobic than GEM, show markedly different values of the diffusion coefficient and, most notably, an inversion in the diffusion trends with χ between acetyl and butanoyl modifications. In acetylated-chitosan networks, DOX diffusion decreases as χ increases, independent of the modification pattern (Figure 7b). However, the network structure and pore size distributions between acetylated-chitosan networks with evenly spaced and blocky modification were the same (Figure 6a,b), ruling out a role of network morphology on decreasing the mobility of DOX as χ increases. Rather, the lower diffusion coefficient of DOX at higher χ is due to a higher number of nonbonded interactions between DOX and the acetyl groups

DOI: 10.1021/acs.biomac.9b00707
Biomacromolecules 2019, 20, 3126−3141

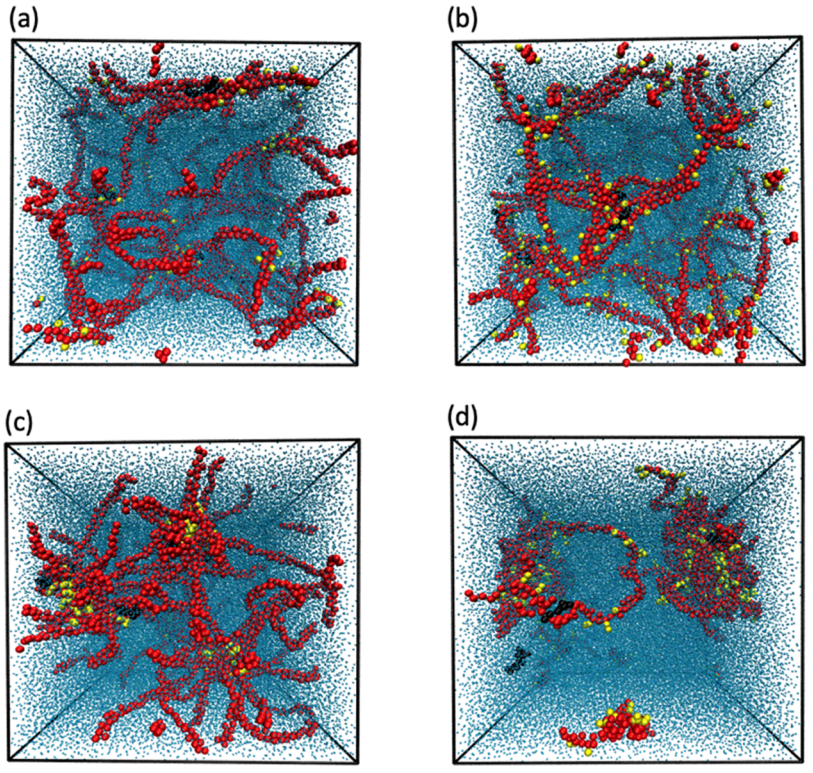

Figure 8. Snapshot of DOX migration through (a) acetyl-chitosan networks at low χ (16%), (b) acetyl-chitosan networks at high χ (50%), (c) butanoyl-chitosan network at low χ (16%), and (d) butanoyl-chitosan networks at high χ (32%), where the chitosan backbone is represented by red beads, modifications are represented by yellow beads, and DOX is represented by black beads.

on the chitosan chains. As reported in Table S1, in fact, the number of nonbonded interactions between DOX and the acetyl moieties increases with χ for both modification patterns, although the number of nonbonded interactions with the backbone remains constant; for example, a DOX molecule forms an average of 15 ± 2 interactions with acetyl-chitosan at χ = 16% and up to 60 ± 4 interactions with acetyl-chitosan at χ = 50% with an evenly spaced pattern. This indicates that hydrophobic nonbonded interactions are the main cause of the slowed diffusion.

DOX diffusion through butanoyl-chitosan gels, on the other hand, increases with χ independent of modification patterns (Figure 7d). As χ increases, the butanoyl-chitosan network undergoes a transition from homogeneous (Figure 4c) to cluster/channel morphology (Figure 4d). Coarse-grained simulations of DOX migration through butanoyl-chitosan networks showed sharp differences in the migration of DOX molecules across chitosan networks with different morphologies. Specifically, the migration of DOX through the homogeneous butanoyl-chitosan network (low χ, Figure 8c) is identical to that of DOX through the homogeneous acetyl-chitosan network (low and high χ, Figure 8a,b). In clustered butanoyl-chitosan, instead, DOX molecules either adsorb onto/within the chitosan clusters or travel freely through the large pores (Figure 8d). This indicates that, as in acetyl-chitosan systems, a high number of interactions occur between DOX and butanoyl-chitosan at high χ (Table S1); at the same time, the DOX molecules freely migrating through the large pore determine a strong increase in the overall diffusion coefficients, as indicated by the comparison in mean-squared displacement (MSD) vs time for both adsorbed and freely migrating DOX molecules (Figure S6). It is also crucial to note that the chitosan vs water ratio and—consequently—the channel vs cluster ratio are much higher in the experimental systems than in the simulated networks. We therefore expect the actual hydrogel to mirror the increase in the diffusion coefficient with χ observed in the coarse-grained simulations.

The faster dynamics enabled by the smoother energy landscapes featured in coarse-grained simulations may introduce some error in the calculation of the diffusion constants; however, the comparison among the migration of drug molecules in different networks provides a reliable evaluation of the influence of the network morphology and physicochemical properties on drug transport. In the cluster/channel morphology, in particular, the difference between diffusional pathways of single-drug molecules becomes very pronounced, with drug molecules experiencing sharper differences in the morphology of the medium through which they diffuse. Collectively, these single-drug simulations indicate that the hydrophobicity driven morphing of the hydrogel structure affects drug diffusion by two opposing mechanisms: first, the larger pores favor the migration of the drug molecules; and second, the nesting of the modification groups within the core of the clusters is responsible for strong adsorption of the drug molecules that collide with the chitosan clusters; notably, our simulations indicate that while both DOX and GEM are affected by the first mechanism, only DOX undergoes the second mechanism. We anticipate that the high water/polymer ratio of the real chitosan hydrogels makes the first mechanism dominant over the second.

Simulation of Dual-Drug Migration through Modified Chitosan Hydrogels. We finally sought to understand how the combination of multiple drugs affects the molecular interactions and diffusion through the networks for different

DOI: 10.1021/acs.biomac.9b00707
Biomacromolecules 2019, 20, 3126−3141

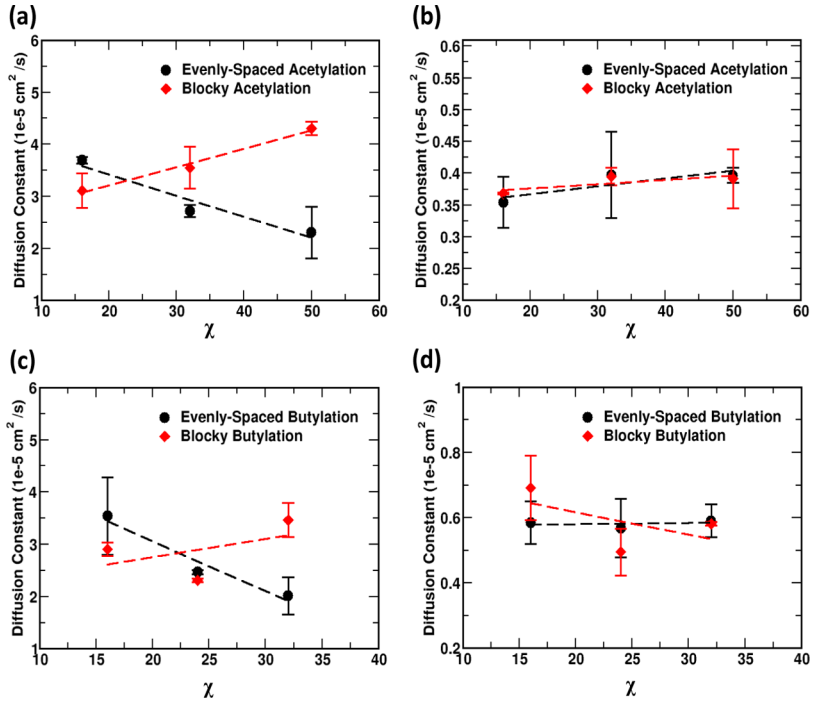

Figure 9. Drug diffusion constants vs χ for dual-drug migration across different chitosan networks: (a) GEM in acetyl-chitosan, (b) DOX in acetyl-chitosan, (c) GEM in butanoyl-chitosan, and (d) DOX in butanoyl-chitosan.

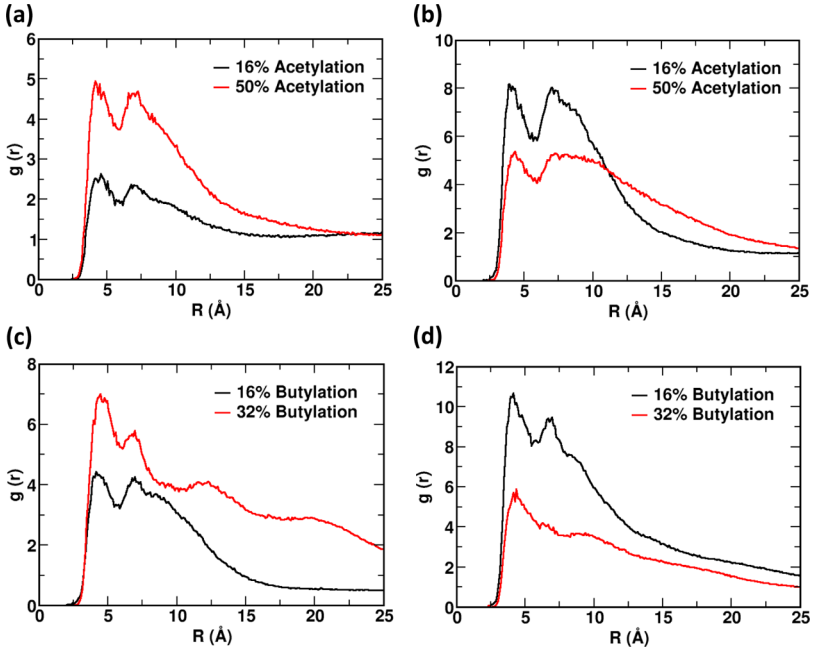

Figure 10. Radial distribution functions of GEM around the center of mass of DOX in acetyl-chitosan networks with (a) evenly spaced and (b) blocky modification, and in butanoyl-chitosan networks with (c) evenly spaced and (d) blocky modification.

types and degrees of modification. Such understanding is needed to gain control over the kinetics and molar ratio of release when using synergistic drug combinations. While numerous in silico models have been developed to simulate the migration of single drugs through polymer hydrogel networks,[69,70] models for multiple drugs are much less common. Combining drugs, especially with different physicochemical properties, in fact, introduces considerable complexity related to drug−drug interactions and their effect on drug−polymer interactions.

Following the procedure outlined above, we performed coarse-grained simulations of equimolar GEM and DOX migration through the different chitosan networks and calculated the diffusion constants for both drugs. Notably, the values derived from dual-drug release (Figure 9) show rather different trends from those obtained with single drugs (Figure 9). In particular, the diffusion of DOX remains almost constant across the entire range of χ for both acetyl- and butanoyl-chitosan. The diffusion of GEM is also markedly different. With an evenly spaced modification pattern, GEM

DOI: 10.1021/acs.biomac.9b00707
Biomacromolecules 2019, 20, 3126−3141

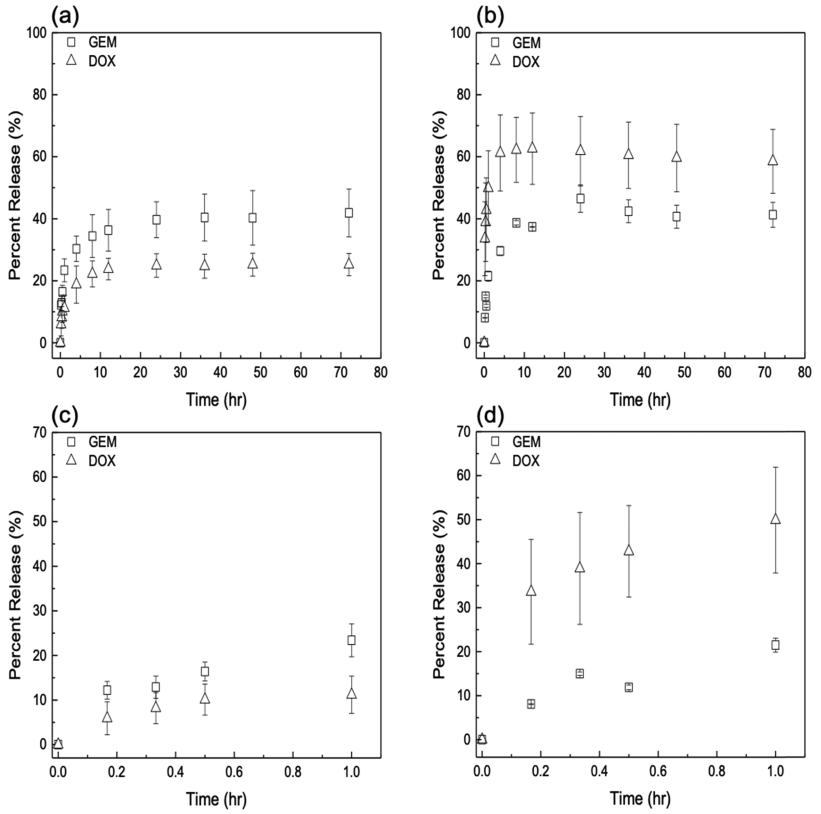

Figure 11. Release profiles of DOX (triangles) and GEM (squares) from chitosan hydrogels at χ = 25% of (a) acetyl at 72 h, and (b) butanoyl at 72 h, (c) acetyl at 1 h, and (d) butanoyl at 1 h. Data represent mean ± 99% CI ($n \geq 3$).

diffusion decreases with χ through both acetyl- and butanoyl-chitosan. With the blocky modification pattern, instead, GEM diffusion increases with χ through acetyl-chitosan and is almost constant with χ through butanoyl-chitosan. These differences are actually the result of drug−drug interactions, which significantly affect drug−polymer interactions. This is confirmed by the radial distribution functions for GEM around DOX molecules, which indicate a strong tendency of the two drug molecules to aggregate. As can be seen from the double-peak shape of the curves in Figure 10, in fact, clusters comprising one DOX and two GEM molecules are frequently formed.

Experimental Single-Drug Release. *Kinetic Profiles of Single-Drug Release.* Single-drug release experiments were performed by contacting 150 mg of drug-loaded hydrogel with PBS at pH 7.4 to simulate physiological conditions. The drug release profiles presented in Figure 11 were obtained using acetyl- and butanoyl-chitosan gels with χ of 25%, which is comparable to the lowest modification investigated in the MD simulations. The analogous plot for heptanoyl-chitosan is reported in Figure S7, and all of the other release profiles for different modification types and degree are reported in Figures S8−S10. Collectively, these data indicate that the choice of modification has a profound impact on the kinetics of drug release.

In the acetyl-chitosan gel (Figure 11a,c), GEM is released slightly more rapidly than DOX, achieving 20% release in about 1 h, compared with 6.5 h for DOX. Notably, the two drugs are released at different doses; in particular, the hydrogels released ∼40% of the GEM payload (100 μg) and ∼25% of the loaded DOX (32 μg) over 72 h, corresponding to a molar ratio of 6.3 of GEM/DOX. The difference in both release kinetics and dose can be related to the physicochemical properties of the two drugs, DOX being moderately hydrophobic and GEM being very hydrophilic. These results agree with the simulations of single-drug diffusion through acetyl-chitosan, wherein the hydrophobic interactions between DOX and the acetyl moieties displayed throughout the homogeneous network decrease its migration compared with GEM, which exhibits no change in the diffusion coefficient as modification prevalence increases in the acetyl-chitosan network (Figure 7a,b).

The butanoyl-chitosan hydrogel shows a markedly different behavior (Figure 11b,d), with DOX being released more rapidly than GEM, reaching 20% release instantaneously compared with 1 h for GEM. Additionally, the hydrogels released ∼45% of the GEM payload (98 μg) and ∼60% of the DOX payload (78 μg) over a 72 h period, corresponding to a molar ratio of 2.6 of GEM/DOX. These results corroborate the single-drug diffusion simulations through the butanoyl-chitosan networks (Figure 7c,d), which indicated that the release of DOX is not affected by LJ-type interactions with the modified chitosan chains, but is rather governed by rapid migration through the large channels produced by the hydrophobic clustering of the butanoyl-chitosan chains. The release of GEM, on the other hand, is unaffected by the transition of a homogenous to heterogeneous structure. Both the computational (Figure 7a,c) and experimental (Figure 10a,b) results of drug diffusion indicate that there is no dependence of GEM diffusion on modification type and pattern. The release profiles of DOX and GEM obtained from chitosan hydrogels constructed with different degrees of acetylation (15−55%) (Figure S8) and butanoation (15−40%) (Figure S9) consistently align with the in silico results,

DOI: 10.1021/acs.biomac.9b00707
Biomacromolecules 2019, 20, 3126−3141

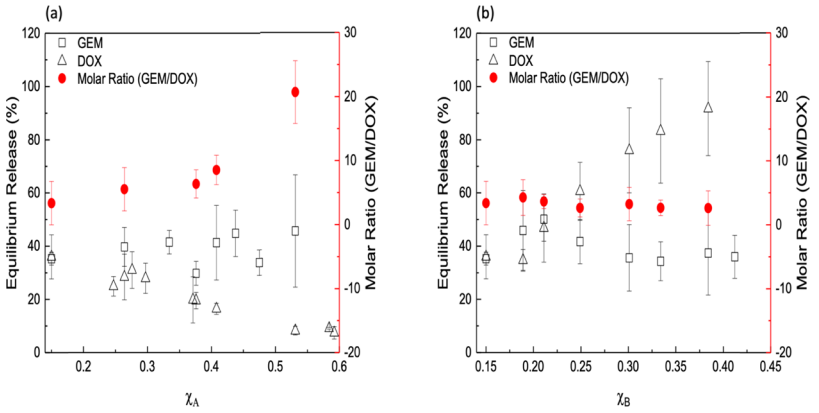

Figure 12. Equilibrium release percents of DOX (triangles) and GEM (squares) and GEM/DOX molar ratio (red circles) vs χ for (a) acetyl-chitosan and (b) butanoyl-chitosan. Data represent mean ± 99% CI ($n \geq 3$).

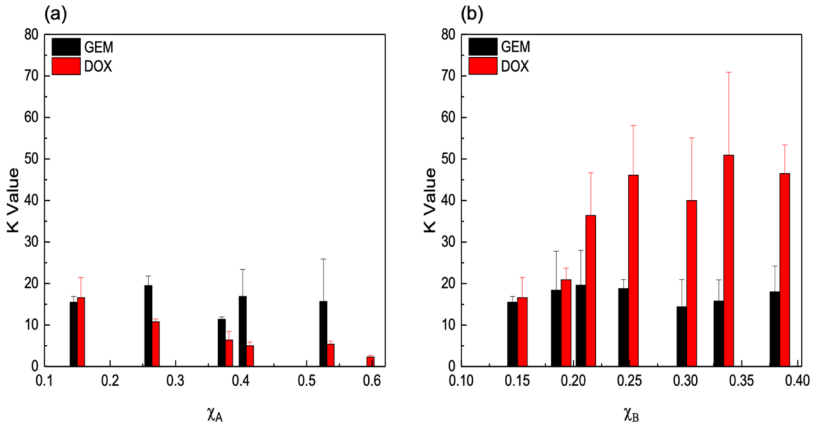

Figure 13. *K* values obtained from the Korsmeyer−Peppas model for single GEM (black) and DOX (red) release vs χ in (a) acetyl-modified chitosan gels and (b) butanoyl-modified chitosan gels. Data represent mean ± 99% CI ($n \geq 3$).

corroborating the correlation between drug release kinetics and hydrophobicity driven morphing of the hydrogel microstructure provided by our coarse-grained model. Drug release from heptanoyl-chitosan gels across a range of χ between 15 and 35% (Figure S10) showed strong similarity with that from butanoyl-chitosan gels. These results were anticipated, given than heptanoyl moieties, owing to their higher hydrophobicity, are expected to trigger the formation of the cluster-channels microstructure at low degrees of modification.

Equilibrium Single-Drug Release. The values of equilibrium release, defined to be the asymptotic values of drug release (t > 30 h), and the corresponding GEM/DOX molar ratio from the different acetyl- and butanoyl-modified gels are collated in Figure 12, where they are plotted against the degree of acetyl and butanoyl modification (χ_A and χ_B). Analogous plots obtained with heptanoyl-modified gels are reported in Figure S11.

For acetyl-modified gels (Figure 12a), a downward trend in DOX release is observed as χ increases, from a 36% release (native chitosan, χ_A = 0.150) to a 7% release (χ_A = 0.592). This is indicative of DOX retention in the hydrogel network by hydrophobic adsorption of the drug on the acetyl modifications (Table S1), as the hydrogel maintains a homogenous structure. The release of GEM fluctuates between 35% release (χ_A = 0.150) and 46% release (χ_A = 0.531), indicating a quasi-constant release within experimental error. The hydrophilic character of GEM minimized its nonbonded interaction with the acetyl moieties (Table S1), rendering its diffusion independent of χ. In butanoyl-chitosan gels (Figure 12b), the amount of DOX released increases significantly with χ, from a 36% release (χ_B = 0.150) to a 92% release (χ_B = 0.384), whereas GEM release remains relatively constant, varying from a 35% release (χ_B = 0.150) to a 36% release (χ_B = 0.411) with no statistically significant difference across all modifications.

These trends fully agree with the results obtained from the single-drug diffusion simulations (Figure 7), indicating that the migration of DOX is controlled by the hydrophobic interactions with the acetyl-chitosan chains arranged in a homogeneous gel and by pure diffusion across the cluster/channels structure of butanoyl-chitosan gels. The migration of GEM, instead, is effectively independent of gel modification and microstructure, likely a result of GEM's hydrophilicity. As discussed above, the trend of DOX release seems to corroborate the hypothesis of a blocky modification pattern, wherein the clusters feature a micellar structure comprising a hydrophobic core rich in butanoyl-chitosan segments and a hydrophilic shell formed by unmodified chitosan segments. In this scenario, in fact, DOX migrates more rapidly than in the case of chitosan modified by evenly spaced modification, where the surface of clusters may display butanoyl groups that would adsorb DOX, thereby hindering its migration.

Mathematical Model Fitting. Drug release data from acetyl-, butanoyl-, and heptanoyl-modified gels loaded with either GEM or DOX were fitted to several empirical models,

DOI: 10.1021/acs.biomac.9b00707
Biomacromolecules 2019, 20, 3126−3141

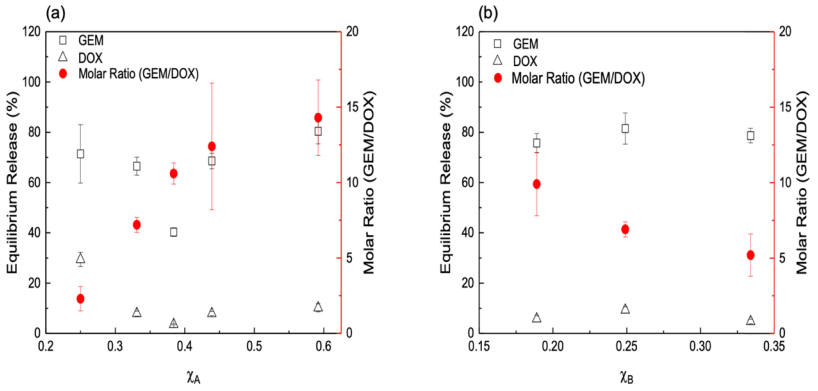

Figure 14. Equilibrium dual-drug release percents of DOX (black triangles) and GEM (black squares), and GEM/DOX molar ratio (red circles) vs χ for (a) acetyl-chitosan and (b) butanoyl-chitosan. Data represent mean ± 99% CI ($n \geq 3$).

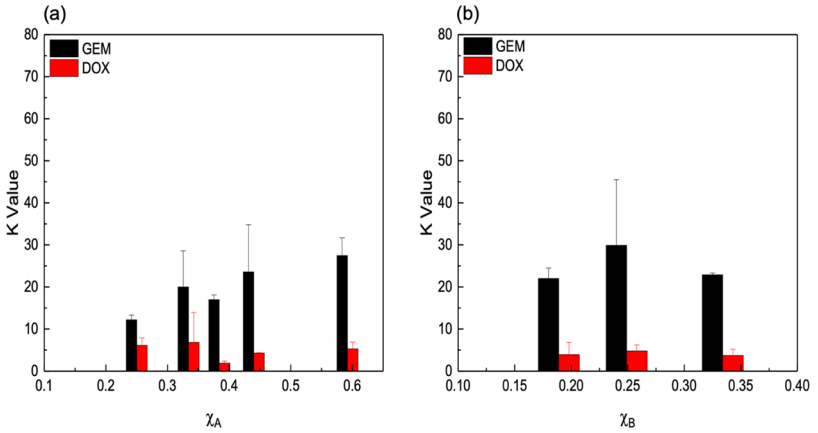

Figure 15. *K* values obtained from the Korsmeyer−Peppas model for GEM (black) and DOX (red) released vs χ from (a) acetyl-modified chitosan gels and (b) butanoyl-chitosan gels. Data represent mean ± 99% CI ($n \geq 3$).

listed in Table S2. The fitting results summarized in Tables S3−S5 indicate that the Korsmeyer−Peppas model provided the best fit for the release of both DOX and GEM from the hydrogels utilized in this study. In the Korsmeyer−Peppas model, the values of the diffusion (or release) exponent n and the kinetic constant *K* are correlated to the mechanism of release and the diffusion coefficient, respectively.[42] In particular, $n \leq 0.45$ indicates a classical Fickian diffusion mechanism from cylindrical matrices. The fitted values of these parameters for acetyl- and butanoyl-chitosan gels are reported in Tables S6 and S7, respectively. For all of the gels, release of DOX and GEM followed the Fickian mechanism.

Notably, the data indicate a clear trend for the release exponent *K* (Figure 13), which is linked to the diffusion coefficient. In acetyl-modified gels (Figure 13a), the *K* values for GEM fluctuate between 11.4 and 19.5, without a strong correlation to χ. The *K* values for DOX, on the other hand, drastically decrease from 16.6 to 2.3 with increasing χ. This translates in a decrease of the effective diffusion coefficient of DOX with χ, due to the increasing number of nonbonded interactions between DOX and the modified chitosan chains at higher χ_A as predicted by our in silico model (Table S1).

The butanoyl-modified gels also showed values of $n \leq 0.45$ for both drugs, indicating a purely Fickian diffusion mechanism of migration through the hydrogel. As with acetyl-modified gels, the values of *K* for GEM release from butanoyl-modified gels fluctuate between 15.8 and 18.8, showing no correlation with χ (Figure 13b). In contrast, the value of *K* for DOX doubles over the range of χ, going from 20.9 to 50.8. As χ increases, in fact, the butanoyl moieties morph the hydrogel structure from a homogeneous network to a heterogeneous cluster/channel structure. Once again, as hypothesized for the blocky modification pattern, the large channels and the concealment of the hydrophobic modifications within the clusters result in a doubling of the effective diffusion coefficient of DOX.

Experimental Dual-Drug Release. The final goal of this study is to develop a delivery system that releases multiple chemotherapeutics with precise kinetics and a molar ratio conducive to synergistic therapeutic effects. We therefore performed a number of dual-drug release studies aimed at correlating the release kinetics and doses of GEM and DOX with the type and degree of modification of the chitosan hydrogel. As in the single-drug studies, dual-drug release was performed using acetyl-, butanoyl-, and heptanoyl-modified gels spanning a range of modification levels comparable to those utilized in the dual-drug in silico modeling. Specifically, acetyl-chitosan gels covered the range of χ values between 0.249 and 0.592, whereas butanoyl-chitosan gels covered a range between 0.189 and 0.334. The resulting release profiles (% release vs time) are reported in Figures S12−S14.

In all dual-drug release studies, the asymptotic release was obtained within 24 h, resulting in wide ranges of equilibrium GEM/DOX molar ratios for both acetyl-chitosan and butanoyl-chitosan gels, as shown in Figure 14. In acetyl-chitosan gels, the equilibrium GEM/DOX molar ratio

DOI: 10.1021/acs.biomac.9b00707
Biomacromolecules 2019, 20, 3126−3141

increases with χ from 2.2 at χ_A = 0.264 to 14.3 at χ_A = 0.592. In butanoyl-chitosan gels, the GEM/DOX ratio decreases with χ, from 10.0 at χ_B = 0.189 to 5.2 at χ_B = 0.334. These trends show some similarity with single-drug release data, although the GEM/DOX ratios are considerably higher for dual-drug release than for the single-drug release.

In addition to equilibrium data, kinetic release properties were determined by fitting the GEM and DOX release data to the Korsmeyer−Peppas model, reported for both acetyl- and butanoyl-chitosan in Figure 15. It is important to notice that the diffusion rate for DOX is nearly constant across the entire range of χ for both acetyl- and butanoyl-chitosan, whereas the GEM diffusion rate slightly increases with χ through acetyl-chitosan and is almost constant with χ through butanoyl-chitosan. These results match the dual-drug release profile predicted by our MD simulations (Figure 9) for chitosan modified with a blocky pattern, thereby corroborating the hypothesis of blocky modification. For both acetyl- and butanoyl- modified gels, the K values for GEM and DOX do not show a strong correlation with χ, likely due to the drug−drug interactions within the chitosan matrix, which are also predicted by the MD simulations (Figure 10). Nonetheless, as observed in single-drug release studies, the releases of GEM and DOX were characterized by markedly different values of K, indicating that GEM is released more rapidly than DOX.

These dual-drug studies demonstrate the efficacy of modified chitosan gels for combined chemotherapeutic treatment. First, the formulations studied herein afford the desired schedule, with GEM being released prior to DOX; in all dual-drug studies, in fact, the ratio of K values (GEM/DOX) ranges from 2.0 to 9.0, with a mean of 5.4, indicating release of GEM much faster than DOX. Second, the desired molar ratio (dose), namely, the molar ratio yielding the highest synergy (GEM/DOX = ∼10), is present from 32 to 42% modification in acetyl-modified gels and from for 19 to 24% modification in butanoyl-modified gels. These findings are consistent with the current literature demonstrating that the combination of GEM and DOX can be administered such that a synergistic efficacy may be observed in vitro or in vivo when the aforementioned kinetics and dose are present.[7,41]

CONCLUSIONS

Hydrogels constructed with native or modified polysaccharides and loaded with chemotherapeutic drugs have been extensively studied, and a number of them have entered the clinical pipeline through the last decade.[71−74] A growing body of literature focuses on polymer conjugates and hydrogels that deliver synergistic combinations of drugs. In developing these systems for a given drug combination, the choice of the modification groups, degree of modification, and initial drug loading are crucial to ensure the therapeutic efficacy of the formulation. Empirical exploration of such a wide design space, however, is cumbersome and hinders the preclinical stages. This study focuses on developing a computationally designed and experimentally validated system that could serve as a powerful guide to pharmaceutical chemists in the identification of the design parameters that afford a schedule and a ratio of drug release that ensure a successful therapeutic outcome. Specifically, the proposed model has managed to accurately portray complex phenomena, such as the different microscale morphologies present in hydrogels constructed with different types and degrees of modification, and the migration of not only one but also two drugs through these modified polymer networks. The experimental data validate the behaviors predicted by the molecular dynamics simulations and indicate specific formulations that afford synergistic combinations for the specific drug pair considered in this study (DOX and GEM) within the scope of the current literature. While focusing on hydrophobically modified chitosan hydrogels and the GEM−DOX drug pair, this method is applicable to any other polymer substrates, whether natural or synthetic, modification moiety, and therapeutic payload. The results presented in this work fully demonstrate the potential of this approach to accelerate the translation of drug-loaded hydrogels for cancer therapy.

ASSOCIATED CONTENT

Supporting Information

The Supporting Information is available free of charge on the ACS Publications website at DOI: 10.1021/acs.biomac.9b00707.

Interaction energies and hydrogen-bond contacts between drug and chitosan chains, comparison between all-atom and coarse-grained simulation radial distribution functions, structures of simulated acetylated and butanoated chitosan networks, full release profiles of acetyl-, butanoyl-, and heptanoyl-modified chitosan hydrogels, mathematical models used to fit release profiles, Korsmeyer−Peppas fits to release profiles, and dual-drug molar ratio release profiles (PDF)

AUTHOR INFORMATION

Corresponding Authors

*E-mail: andrea.grafmueller@mpikg.mpg.de (A.G.).
*E-mail: smenega@ncsu.edu (S.M.).

ORCID

Carol K. Hall: 0000-0002-7425-587X
Andrea Grafmüller: 0000-0002-1671-3158

Author Contributions

§J.D.S. and A.S. contributed equally to this work.

Author Contributions

The manuscript was written through contributions of all authors. All authors have given approval to the final version of the manuscript.

Notes

The authors declare no competing financial interest.

ACKNOWLEDGMENTS

This work was funded by start-up funds provided by NC State University. S.M. and J.D.S. kindly acknowledge support from the Department of Education Graduate Assistance in Areas of National Need (GAANN) Fellowship in Molecular Biotechnology. A.G. and A.S. kindly acknowledge support from the Deutsche Forschungsgemeinschaft International Research Training group (IRTG 1524). C.K.H. acknowledges NSF CBET-1743432.

REFERENCES

(1) Zhang, D.; Fan, D. New Insights into the Mechanisms of Gastric Cancer Multidrug Resistance and Future Perspectives. *Future Oncol.* **2010**, *6*, 527−537.

(2) Saeki, T.; Tsuruo, T.; Sato, W.; Nishikawsa, K. Drug Resistance in Chemotherapy for Breast Cancer. *Cancer Chemother. Pharmacol.* **2005**, *56*, 84−89.

DOI: 10.1021/acs.biomac.9b00707
Biomacromolecules 2019, 20, 3126−3141

(3) Frączek, N.; Bronisz, I.; Pietryka, M.; Kępińska, D.; Strzała, P.; Mielnicka, K.; Korga, A.; Dudka, J. An Outline of Main Factors of Drug Resistance Influencing Cancer Therapy. *J. Chemother.* **2016**, *28*, 457−464.
(4) Lotfi-Jam, K.; Carey, M.; Jefford, M.; Schofield, P.; Charleson, C.; Aranda, S. Nonpharmacologic Strategies for Managing Common Chemotherapy Adverse Effects: A Systematic Review. *J. Clin. Oncol.* **2008**, *26*, 5618−5629.
(5) Genre, D.; Protière, C.; Macquart-Moulin, G.; Gravis, G.; Camerlo, J.; Alzieu, C.; Maraninchi, D.; Moatti, J.-P.; Viens, P. Quality of Life of Breast Cancer Patients Receiving High-Dose-Intensity Chemotherapy: Impact of Length of Cycles. *Support Care Cancer* **2002**, *10*, 222−230.
(6) Chou, T.-C. Drug Combination Studies and Their Synergy Quantification Using the Chou-Talalay Method. *Cancer Res.* **2010**, *70*, 440−446.
(7) Vogus, D. R.; Evans, M. A.; Pusuluri, A.; Barajas, A.; Zhang, M.; Krishnan, V.; Nowak, M.; Menegatti, S.; Helgeson, M. E.; Squires, T. M.; Mitragotri, S. A Hyaluronic Acid Conjugate Engineered to Synergistically and Sequentially Deliver Gemcitabine and Doxorubicin to Treat Triple Negative Breast Cancer. *J. Controlled Release* **2017**, *267*, 191−202.
(8) Rui, M.; Xin, Y.; Li, R.; Ge, Y.; Feng, C.; Xu, X. Targeted Biomimetic Nanoparticles for Synergistic Combination Chemotherapy of Paclitaxel and Doxorubicin. *Mol. Pharmaceutics* **2017**, *14*, 107−123.
(9) Li, T.; Ling, Y.-H.; Goldman, I. D.; Perez-Soler, R. Schedule-Dependent Cytotoxic Synergism of Pemetrexed and Erlotinib in Human Non-Small Cell Lung Cancer Cells. *Clin. Cancer Res.* **2007**, *13*, 3413−3422.
(10) Meczes, E. L.; Pearson, A. D. J.; Austin, C. A.; Tilby, M. J. Schedule-Dependent Response of Neuroblastoma Cell Lines to Combinations of Etoposide and Cisplatin. *Br. J. Cancer* **2002**, *86*, 485−489.
(11) Hu, Q.; Sun, W.; Wang, C.; Gu, Z. Recent Advances of Cocktail Chemotherapy by Combination Drug Delivery Systems. *Adv. Drug Delivery Rev.* **2016**, *98*, 19−34.
(12) Camacho, K. M.; Menegatti, S.; Mitragotri, S. Low-Molecular-Weight Polymer-Drug Conjugates for Synergistic Anticancer Activity of Camptothecin and Doxorubicin Combinations. *Nanomedicine* **2016**, *11*, 1139−1151.
(13) Zhang, Y.; Yang, C.; Wang, W.; Liu, J.; Liu, Q.; Huang, F.; Chu, L.; Gao, H.; Li, C.; Kong, D.; Liu, Q.; Liu, J. Co-Delivery of Doxorubicin and Curcumin by PH-Sensitive Prodrug Nanoparticle for Combination Therapy of Cancer. *Sci. Rep.* **2016**, *6*, No. 21225.
(14) Huang, W.-T.; Larsson, M.; Lee, Y.-C.; Liu, D.-M.; Chiou, G.-Y. Dual Drug-Loaded Biofunctionalized Amphiphilic Chitosan Nanoparticles: Enhanced Synergy between Cisplatin and Demethoxycurcumin against Multidrug-Resistant Stem-like Lung Cancer Cells. *Eur. J. Pharm. Biopharm.* **2016**, *109*, 165−173.
(15) Camacho, K. M.; Menegatti, S.; Vogus, D. R.; Pusuluri, A.; Fuchs, Z.; Jarvis, M.; Zakrewsky, M.; Evans, M. A.; Chen, R.; Mitragotri, S. DAFODIL: A Novel Liposome-Encapsulated Synergistic Combination of Doxorubicin and 5FU for Low Dose Chemotherapy. *J. Controlled Release* **2016**, *229*, 154−162.
(16) Zhang, B.; Wang, T.; Yang, S.; Xiao, Y.; Song, Y.; Zhang, N.; Garg, S. Development and Evaluation of Oxaliplatin and Irinotecan Co-Loaded Liposomes for Enhanced Colorectal Cancer Therapy. *J. Controlled Release* **2016**, *238*, 10−21.
(17) Scarano, W.; de Souza, P.; Stenzel, M. H. Dual-Drug Delivery of Curcumin and Platinum Drugs in Polymeric Micelles Enhances the Synergistic Effects: A Double Act for the Treatment of Multidrug-Resistant Cancer. *Biomater. Sci.* **2014**, *3*, 163−174.
(18) Zhang, P.; Li, J.; Ghazwani, M.; Zhao, W.; Huang, Y.; Zhang, X.; Venkataramanan, R.; Li, S. Effective Co-Delivery of Doxorubicin and Dasatinib Using a PEG-Fmoc Nanocarrier for Combination Cancer Chemotherapy. *Biomaterials* **2015**, *67*, 104−114.
(19) Zhou, D.; Xiao, H.; Meng, F.; Li, X.; Li, Y.; Jing, X.; Huang, Y. A Polymer−(Tandem Drugs) Conjugate for Enhanced Cancer Treatment. *Adv. Healthcare Mater.* **2013**, *2*, 822−827.
(20) Li, X.; Fan, R.; Wang, Y.; Wu, M.; Tong, A.; Shi, J.; Xiang, M.; Zhou, L.; Guo, G. In Situ Gel-Forming Dual Drug Delivery System for Synergistic Combination Therapy of Colorectal Peritoneal Carcinomatosis. *RSC Adv.* **2015**, *5*, 101494−101506.
(21) Wu, X.; He, C.; Wu, Y.; Chen, X. Synergistic Therapeutic Effects of Schiff's Base Cross-Linked Injectable Hydrogels for Local Co-Delivery of Metformin and 5-Fluorouracil in a Mouse Colon Carcinoma Model. *Biomaterials* **2016**, *75*, 148−162.
(22) Huang, J.; Wang, W.-J.; Li, B.-G.; Zhu, S. Design and Synthesis of Poly(Butyl Acrylate) Networks through RAFT Polymerization with Crosslinking for Controlled-Release Applications. *Macromol. Mater. Eng.* **2013**, *298*, 391−399.
(23) Hezaveh, H.; Muhamad, I. I. Modification and Swelling Kinetic Study of Kappa-Carrageenan-Based Hydrogel for Controlled Release Study. *J. Taiwan Inst. Chem. Eng.* **2013**, *44*, 182−191.
(24) Hoare, T. R.; Kohane, D. S. Hydrogels in Drug Delivery: Progress and Challenges. *Polymer* **2008**, *49*, 1993−2007.
(25) Li, J.; Mooney, D. J. Designing Hydrogels for Controlled Drug Delivery. *Nat. Rev. Mater.* **2016**, *1*, No. 16071.
(26) Bhattarai, N.; Gunn, J.; Zhang, M. Chitosan-Based Hydrogels for Controlled, Localized Drug Delivery. *Adv. Drug Delivery Rev.* **2010**, *62*, 83−99.
(27) Hu, L.; Sun, Y.; Wu, Y. Advances in Chitosan-Based Drug Delivery Vehicles. *Nanoscale* **2013**, *5*, 3103−3111.
(28) Riva, R.; Ragelle, H.; des Rieux, A.; Duhem, N.; Jérôme, C.; Préat, V. Chitosan and Chitosan Derivatives in Drug Delivery and Tissue Engineering. In *Chitosan for Biomaterials II*; Jayakumar, R., Prabaharan, M., Muzzarelli, R. A. A., Eds.; Springer: Berlin, Heidelberg, 2011; pp 19−44.
(29) Peppas, N. A.; Hilt, J. Z.; Khademhosseini, A.; Langer, R. Hydrogels in Biology and Medicine: From Molecular Principles to Bionanotechnology. *Adv. Mater.* **2006**, *18*, 1345−1360.
(30) Nur, M.; Vasiljevic, T. Can Natural Polymers Assist in Delivering Insulin Orally? *Int. J. Biol. Macromol.* **2017**, *103*, 889−901.
(31) Hong, S.-C.; Yoo, S.-Y.; Kim, H.; Lee, J. Chitosan-Based Multifunctional Platforms for Local Delivery of Therapeutics. *Mar. Drugs* **2017**, *15*, No. 60.
(32) Lam, P. L.; Gambari, R. Advanced Progress of Microencapsulation Technologies: In Vivo and in Vitro Models for Studying Oral and Transdermal Drug Deliveries. *J. Controlled Release* **2014**, *178*, 25−45.
(33) Perilla, J. R.; Goh, B. C.; Cassidy, C. K.; Liu, B.; Bernardi, R. C.; Rudack, T.; Yu, H.; Wu, Z.; Schulten, K. Molecular Dynamics Simulations of Large Macromolecular Complexes. *Curr. Opin. Struct. Biol.* **2015**, *31*, 64−74.
(34) Katiyar, R. S.; Jha, P. K. Molecular Simulations in Drug Delivery: Opportunities and Challenges. *Wiley Interdiscip. Rev.: Comput. Mol. Sci.* **2018**, *8*, No. e1358.
(35) Albano, J. M. R.; de Paula, E.; Pickholz, M. Molecular Dynamics Simulations to Study Drug Delivery Systems. *Mol. Dyn.* **2018**, 74−90, DOI: 10.5772/intechopen.75748.
(36) Liu, D.; Chen, Y.; Feng, X.; Deng, M.; Xie, G.; Wang, J.; Zhang, L.; Liu, Q.; Yuan, P. Micellar Nanoparticles Loaded with Gemcitabine and Doxorubicin Showed Synergistic Effect. *Colloids Surf., B* **2014**, *113*, 158−168.
(37) Lammers, T.; Subr, V.; Ulbrich, K.; Peschke, P.; Huber, P. E.; Hennink, W. E.; Storm, G. Simultaneous Delivery of Doxorubicin and Gemcitabine to Tumors in Vivo Using Prototypic Polymeric Drug Carriers. *Biomaterials* **2009**, *30*, 3466−3475.
(38) Nahire, R.; Haldar, M. K.; Paul, S.; Ambre, A. H.; Meghnani, V.; Layek, B.; Katti, K. S.; Gange, K. N.; Singh, J.; Sarkar, K.; Mallik, S. Multifunctional Polymersomes for Cytosolic Delivery of Gemcitabine and Doxorubicin to Cancer Cells. *Biomaterials* **2014**, *35*, 6482−6497.
(39) Croissant, J. G.; Zhang, D.; Alsaiari, S.; Lu, J.; Deng, L.; Tamanoi, F.; AlMalik, A. M.; Zink, J. I.; Khashab, N. M. Protein-Gold Clusters-Capped Mesoporous Silica Nanoparticles for High Drug

DOI: 10.1021/acs.biomac.9b00707
Biomacromolecules 2019, 20, 3126−3141

Loading, Autonomous Gemcitabine/Doxorubicin Co-Delivery, and in-Vivo Tumor Imaging. *J. Controlled Release* **2016**, *229*, 183−191.
(40) Ni, S.; Qiu, L.; Zhang, G.; Zhou, H.; Han, Y. Lymph Cancer Chemotherapy: Delivery of Doxorubicin−Gemcitabine Prodrug and Vincristine by Nanostructured Lipid Carriers. *Int. J. Nanomed.* **2017**, *12*, 1565−1576.
(41) Vogus, D. R.; Pusuluri, A.; Chen, R.; Mitragotri, S. Schedule Dependent Synergy of Gemcitabine and Doxorubicin: Improvement of in Vitro Efficacy and Lack of in Vitro-in Vivo Correlation. *Bioeng. Transl. Med.* **2018**, *3*, 49−57.
(42) Korsmeyer, R. W.; Gurny, R.; Doelker, E.; Buri, P.; Peppas, N. A. Mechanisms of Solute Release from Porous Hydrophilic Polymers. *Int. J. Pharm.* **1983**, *15*, 25−35.
(43) Kubota, N.; Tatsumoto, N.; Sano, T.; Toya, K. A Simple Preparation of Half N-Acetylated Chitosan Highly Soluble in Water and Aqueous Organic Solvents. *Carbohydr. Res.* **2000**, *324*, 268−274.
(44) Kaiser, E.; Colescott, R. L.; Bossinger, C. D.; Cook, P. I. Color Test for Detection of Free Terminal Amino Groups in the Solid-Phase Synthesis of Peptides. *Anal. Biochem.* **1970**, *34*, 595−598.
(45) Van Der Spoel, D. V. D.; Lindahl, E.; Hess, B.; Groenhof, G.; Mark, A. E.; Berendsen, H. J. C. GROMACS: Fast, Flexible, and Free. *J. Comput. Chem.* **2005**, *26*, 1701−1718.
(46) Kirschner, K. N.; Yongye, A. B.; Tschampel, S. M.; González-Outeiriño, J.; Daniels, C. R.; Foley, B. L.; Woods, R. J. GLYCAM06: A Generalizable Biomolecular Force Field. Carbohydrates. *J. Comput. Chem.* **2008**, *29*, 622−655.
(47) Sauter, J.; Grafmüller, A. Predicting the Chemical Potential and Osmotic Pressure of Polysaccharide Solutions by Molecular Simulations. *J. Chem. Theory Comput.* **2016**, *12*, 4375−4384.
(48) Case, D. A.; Darden, T. A.; Cheatham, T. E., III; Simmerling, C. L.; Wang, J.; Duke, R. E.; Luo, R.; Crowley, M.; Walker, R. C.; Zhang, W.; Merz, K. M.; Wang, B.; Hayik, S.; Roitberg, A.; Seabra, G.; Kolossváry, I.; Wong, K. F.; Paesani, F.; Vanicek, J.; Wu, X.; Brozell, S. R.; Steinbrecher, T.; Gohlke, H.; Yang, L.; Tan, C.; Mongan, J.; Hornak, V.; Cui, G.; Mathews, D. H.; Seetin, M. G.; Sagui, C.; Babin, V.; Kollman, P. A. *AMBER 10*; University of California: San Francisco, 2008.
(49) Darden, T.; York, D.; Pedersen, L. Particle Mesh Ewald: An N·log(N) Method for Ewald Sums in Large Systems. *J. Chem. Phys.* **1993**, *98*, 10089−10092.
(50) Parrinello, M.; Rahman, A. Polymorphic Transitions in Single Crystals: A New Molecular Dynamics Method. *J. Appl. Phys.* **1981**, *52*, 7182−7190.
(51) Rühle, V.; Junghans, C.; Lukyanov, A.; Kremer, K.; Andrienko, D. Versatile Object-Oriented Toolkit for Coarse-Graining Applications. *J. Chem. Theory Comput.* **2009**, *5*, 3211−3223.
(52) Lu, L.; Izvekov, S.; Das, A.; Andersen, H. C.; Voth, G. A. Efficient, Regularized, and Scalable Algorithms for Multiscale Coarse-Graining. *J. Chem. Theory Comput.* **2010**, *6*, 954−965.
(53) Sauter, J.; Grafmüller, A. Procedure for Transferable Coarse-Grained Models of Aqueous Polysaccharides. *J. Chem. Theory Comput.* **2017**, *13*, 223−236.
(54) Patra, P. K.; Bhattacharya, B. A Deterministic Thermostat for Controlling Temperature Using All Degrees of Freedom. *J. Chem. Phys.* **2014**, *140*, No. 064106.
(55) Nosé, S. A Unified Formulation of the Constant Temperature Molecular Dynamics Methods. *J. Chem. Phys.* **1984**, *81*, 511−519.
(56) Hoover, W. G. Canonical Dynamics: Equilibrium Phase-Space Distributions. *Phys. Rev. A* **1985**, *31*, 1695−1697.
(57) Bhattacharya, S.; Gubbins, K. E. Fast Method for Computing Pore Size Distributions of Model Materials. *Langmuir* **2006**, *22*, 7726−7731.
(58) Kappel, F.; Kuntsevich, A. V. An Implementation of Shor's r-Algorithm. *Comput. Optim. Appl.* **2000**, *15*, 193−205.
(59) Dash, S.; Murthy, P. N.; Nath, L.; Chowdhury, P. Kinetic Modeling on Drug Release from Controlled Drug Delivery Systems. *Acta Pol. Pharm.* **2010**, *67*, 217−223.
(60) Hixson, A. W.; Crowell, J. H. Dependence of Reaction Velocity upon Surface and Agitation. *Ind. Eng. Chem.* **1931**, *23*, 923−931.
(61) Higuchi, T. Mechanism of Sustained-Action Medication. Theoretical Analysis of Rate of Release of Solid Drugs Dispersed in Solid Matrices. *J. Pharm. Sci.* **1963**, *52*, 1145−1149.
(62) Ercolessi, F.; Adams, J. B. Interatomic Potentials from First-Principles Calculations: The Force-Matching Method. *Europhys. Lett.* **1994**, *26*, 583−588.
(63) Noid, W. G.; Chu, J.-W.; Ayton, G. S.; Krishna, V.; Izvekov, S.; Voth, G. A.; Das, A.; Andersen, H. C. The Multiscale Coarse-Graining Method. I. A Rigorous Bridge between Atomistic and Coarse-Grained Models. *J. Chem. Phys.* **2008**, *128*, No. 244114.
(64) Lu, L.; Dama, J. F.; Voth, G. A. Fitting Coarse-Grained Distribution Functions through an Iterative Force-Matching Method. *J. Chem. Phys.* **2013**, *139*, No. 121906.
(65) Ortona, O.; D'Errico, G.; Mangiapia, G.; Ciccarelli, D. The Aggregative Behavior of Hydrophobically Modified Chitosans with High Substitution Degree in Aqueous Solution. *Carbohydr. Polym.* **2008**, *74*, 16−22.
(66) Jiang, G.-B.; Quan, D.; Liao, K.; Wang, H. Preparation of Polymeric Micelles Based on Chitosan Bearing a Small Amount of Highly Hydrophobic Groups. *Carbohydr. Polym.* **2006**, *66*, 514−520.
(67) Rinaudo, M.; Auzely, R.; Vallin, C.; Mullagaliev, I. Specific Interactions in Modified Chitosan Systems. *Biomacromolecules* **2005**, *6*, 2396−2407.
(68) Philippova, O. E.; Korchagina, E. V. Chitosan and Its Hydrophobic Derivatives: Preparation and Aggregation in Dilute Aqueous Solutions. *Polym. Sci., Ser. A* **2012**, *54*, 552−572.
(69) Yeh, P. D.; Alexeev, A. Mesoscale Modelling of Environmentally Responsive Hydrogels: Emerging Applications. *Chem. Commun.* **2015**, *51*, 10083−10095.
(70) Decuzzi, P. Facilitating the Clinical Integration of Nanomedicines: The Roles of Theoretical and Computational Scientists. *ACS Nano* **2016**, *10*, 8133−8138.
(71) Svenson, S.; Wolfgang, M.; Hwang, J.; Ryan, J.; Eliasof, S. Preclinical to Clinical Development of the Novel Camptothecin Nanopharmaceutical CRLX101. *J. Controlled Release* **2011**, *153*, 49−55.
(72) Schluep, T.; Hwang, J.; Hildebrandt, I. J.; Czernin, J.; Choi, C. H. J.; Alabi, C. A.; Mack, B. C.; Davis, M. E. Pharmacokinetics and Tumor Dynamics of the Nanoparticle IT-101 from PET Imaging and Tumor Histological Measurements. *Proc. Natl. Acad. Sci. U.S.A.* **2009**, *106*, 11394−11399.
(73) Weiss, G. J.; Chao, J.; Neidhart, J. D.; Ramanathan, R. K.; Bassett, D.; Neidhart, J. A.; Choi, C. H. J.; Chow, W.; Chung, V.; Forman, S. J.; et al. First-in-Human Phase 1/2a Trial of CRLX101, a Cyclodextrin-Containing Polymer-Camptothecin Nanopharmaceutical in Patients with Advanced Solid Tumor Malignancies. *Invest. New Drugs* **2013**, *31*, 986−1000.
(74) Clark, A. J.; Wiley, D. T.; Zuckerman, J. E.; Webster, P.; Chao, J.; Lin, J.; Yen, Y.; Davis, M. E. CRLX101 Nanoparticles Localize in Human Tumors and Not in Adjacent, Nonneoplastic Tissue after Intravenous Dosing. *Proc. Natl. Acad. Sci. U.S.A.* **2016**, *113*, 3850−3854.

DOI: 10.1021/acs.biomac.9b00707
Biomacromolecules 2019, 20, 3126−3141